

RESEARCH

Open Access



Blast Response Simulation of the Alfred Murrah Building Reinforced by Use of HPFRCC

Jae-Wook Jung¹ and Jung-Wuk Hong^{2*}

Abstract

Structural behavior against the blast load is evaluated for a structure reinforced by high-performance fiber-reinforced cementitious composites (HPFRCC). The Alfred P. Murrah Federal Building, which experienced a terrorist attack in 1995 is taken into consideration for the blast analysis using the finite element method. The continuous surface cap model (CSCM) is used to simulate the behavior of normal concrete and HPFRCC. By reinforcing normal concrete with HPFRCC, damage, and deformation of the structure are significantly reduced. This study presents an efficient reinforcement method by performing an explosion simulation on the structure using HPFRCC and evaluating the behavior according to various reinforcement methods. Specific reinforcements according to the types of members are required to enhance the efficiency of reinforcement. With the optimized reinforcement using high-performance fiber-reinforced cementitious composites (HPFRCC), the resistance to blast load is significantly improved.

Keywords: HPFRCC, finite element analysis, blast analysis, Oklahoma city bombing, Alfred Murrah building

1 Introduction

The Alfred Murrah building was the primary target of the 1995 Oklahoma City Bombing. On April 19, 1995, a truck carrying 4000 lb (1812 kg) of TNT exploded, causing almost a third of the building to collapse. This attack was the most destructive terrorist act in the United States until the 9/11 attacks in 2001 (Kazemi-Moghaddam and Sasani 2015). The bombing killed 168 people, including 19 children under the age of six, and injured more than 680 people, resulting in an economic loss of \$ 652 million. Social infrastructure and public facilities also have been exposed to terrorist attacks. Therefore, the safety of structures against accidents and blast loads is becoming an important social issue. Consequently, the demand for structural resistance to impact and blast loads has increased, in addition to the compressional strength that a concrete structure must have (Choi et al. 2014a, b). One

of the materials to meet this need is high-performance fiber-reinforced cementitious composite (HPFRCC), which overcome the limitation of normal concrete in terms of tensile strength, strain, and ductility.

HPFRCC is fiber-reinforced material based on cement to control the progress of cracks in concrete to improve tensile strength and induce ductile fracture. Concrete shows a brittle fracture, and its resistance against compression is stiff, but its tensile performance is weak. Therefore, when a concrete structure is exposed to high pressure, tensile failure occurs at the backside. As an initiative to complement these properties, fiber-reinforced cementitious composite with strain-hardening properties after initial cracking was developed in the early 1990s (Choi et al. 2014a, b; Kosa et al. 1991). In fiber-reinforced concrete, the ductility of the concrete is significantly improved by the bridging effect of the fiber across the crack (Caverzan et al. 2012). In particular, HPFRCC has higher tensile strength and energy absorption capacity than normal fiber-reinforced concrete (FRC), which significantly improves the resistance performance of the structure (Tran and Kim 2014). In addition, unlike concrete, which has been studied a lot in the past, it is difficult to estimate the parameters of material models for

*Correspondence: j.hong@kaist.ac.kr; jwhong@alum.mit.edu

² Department of Civil and Environmental Engineering, Korea Advanced Institute of Science and Technology, 291 Daehak-ro, Yuseong-gu, Daejeon 34141, Republic of Korea

Full list of author information is available at the end of the article
Journal information: ISSN 1976-0485 / eISSN 2234-1315

recently developed materials such as HPFRCC. Recently, studies were conducted to estimate the material model parameters of UHPC material by Liang et al. and Mohammad et al. (Khosravani et al. 2019; Ren et al. 2020). Also, Yin et al. have studied various blast simulations for UHPC material (Yin et al. 2019a, b).

In this study, the blast-resistance performance of a structure reinforced by HPFRCC is evaluated using the finite element method, which is widely used in engineering analysis (Bathe 2006). In particular, the RC structure of the north side of the Alfred Murrah building, which was directly destroyed by the blast load, is constructed, and numerical analyses are carried out using the finite element method. In the Alfred Murrah building, the RC structure, made of normal concrete, is reinforced by HPFRCC step by step to evaluate the efficiency of blast resistance. Research on blast simulations with recently developed materials, HPFRCC, is quite limited. It is very important to numerically predict the blast-resistance capability of civilian structures using the latest materials and to suggest reinforcement methods. In particular, the prediction of blast-resistance effects using the latest materials for civilian damages caused by explosion terrorism, such as the Oklahoma case, has excellent engineering and sociological significance.

2 Material Plasticity

The linear elasticity theory is conveniently used to describe the behavior of materials in a small deformation regime returning to their original configuration when removing external forces applied to the material. However, most practical materials are affected by the plastic deformation that remains deformed even after removing the applied external force. The material reaches the threshold value of the yield stress, then permanent deformation occurs. In the elastic regime, the energy

accumulated during the deformation process of the material is completely recovered after the removal of the external force, whereas if the plastic deformation occurs, permanent deformation remains, and the dissipation of energy occurs.

A CSCM model is widely used for expressing the behavior of concrete reflecting the plasticity regime of the material (Jung et al. 2019). The CSCM model is a cap model in which the shear yield surface and the hardening cap cross each other smoothly (Hallquist 2007). The general shape of the yield surface in two dimensions is shown in Fig. 1 and this surface uses a multiplicative formulation to smoothly and continuously couple the shear and cap surfaces.

The total strain ε is divided into the elastic strain, ε^e , and the plastic part, ε^p as

$$\varepsilon = \varepsilon^e + \varepsilon^p. \tag{1}$$

By equilibrium considerations, the stress with elasticity tensor C is σ , and we have the elastic relationship as

$$\sigma = C : (\varepsilon - \varepsilon^p). \tag{2}$$

After an initial elasticity stage, the concrete may yield and fail according to the stress state. Yield stresses are defined by the yield surface. For each time step, the stress is updated via Hook's law. This updated stress is called the trial elastic stress, and if the state of trial elastic stress state is on or inside the yielding surface, the behavior is elastic, and the plastic algorithm is ignored. If the elastic stress state is outside the yield surface, the behavior is elastic–plastic, and the plastic algorithm returns the stress state to the yield surface. The yield surface function f is a function of three stress invariants and cap hardening parameter κ as

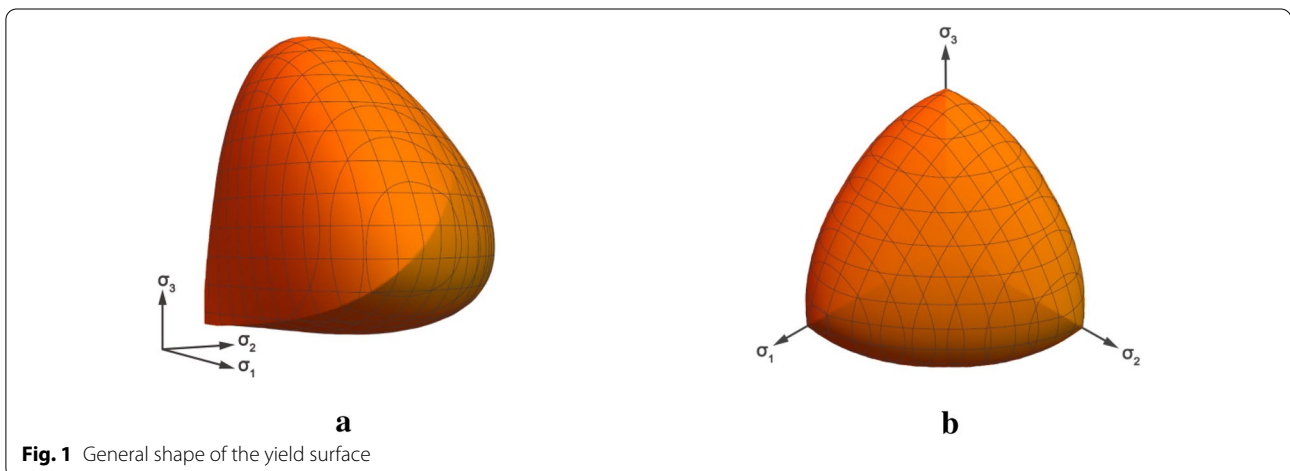


Fig. 1 General shape of the yield surface

$$f(J_1, J_2', J_3', \kappa) = J_2' - \mathfrak{R}^2 F_f^2 F_c, \tag{3}$$

$$J_1 = 3PJ_2' = \frac{1}{2} S_{ij} S_{ij} J_3' = \frac{1}{3} S_{ij} S_{jk} S_{ki}, \tag{4}$$

where J_1 is the first invariant of the stress tensor, J_2' is the second invariant of the deviatoric stress tensor, J_3' is the third invariant of the deviatoric stress tensor, F_f is the shear failure surface, F_c is the hardening cap, \mathfrak{R} is the Rubin scaling function that determines the shape of the intersection between the failure surface and the octahedral plane, P is the pressure, and S_{ij} is the deviatoric stress tensor (Murray 2007). The yield surface in the tensile and low confining pressure region is determined as the shear failure surface, F_f , as

$$F_f(J_1) = \alpha - \lambda \exp(-\beta J_1) + \theta J_1, \tag{5}$$

where the values of α , β , λ , and θ are determined from the triaxial compression (TXC) test. The strength of concrete is typically evaluated as a relationship between principal stress difference versus pressure. The principal stress difference is $(\sigma_a - \sigma_c)$, where σ_a is axial stress and σ_c is confining stress at the TXC stress state (Murray 2007).

The yield surface in the low-to-high confining pressure region is determined as the combination of cap surface (F_c) and shear surface (F_f) as $F_f^2 F_c$. Cap surface, F_c , is expressed as

$$F_c(J_1, \kappa) = 1 - \frac{[J_1 - L(\kappa)][|J_1 - L(\kappa)| + J_1 - L(\kappa)]}{2[X(\kappa) - L(\kappa)]^2}, \tag{6}$$

where $L(\kappa)$ is the functions of κ for determining the intersection of the cap and shear surfaces, and $X(\kappa)$ is the function to define cap ellipticity ratio (Murray 2007).

Specifically, concrete has the property of softening in the state of tensile and low-to-moderate compressive regime. To account for this characteristic, the scalar damage parameter d is used to transform the damaged viscoplastic stress tensor with the deformation stress tensor without damaging it (Eq. (7)). Without the damage formulation, the CSCM model predicts complete plastic behavior based on laboratory tests, but this behavior is not realistic. The accumulation of damage is based on two separate formulas, brittle damage and ductile damage (Eqs. (8) and (9)). The initial damage threshold coincides with the shear yield surface. The damage parameter d increases from the initial value of 0 to the maximum value of 1. When d is equal to 1, the element loses all strength and stiffness. With very low rigidity, the element erosion can be used as an option to avoid computational difficulties. If the element d is greater than 0.99, and the

maximum principal strain is greater than the input variable (1-ERODE), the element is removed.

The damage model describes modulus reduction and softening. Softening is a phenomenon in which the strength decreases after peak strength value. Modulus reduction is a decrease in the slope of loading/unloading curves during cyclic loading. The damage formulation is implemented based on the research of Simo and Ju (1987) as

$$\sigma_{ij}^d = (1 - d)\sigma_{ij}^{vp}, \tag{7}$$

$$\tau_b = \sqrt{E \varepsilon_{max}^2}, \tag{8}$$

$$\tau_d = \sqrt{\frac{1}{2} \sigma_{ij} \varepsilon_{ij}}, \tag{9}$$

where d is damage parameter, σ^{vp} is stress tensor without damage, and σ^d is stress tensor with damage. The damage parameter d varies from 0 (no damage) to 1 (complete damage), and $1 - d$ is a reduction factor based on accumulated damage. Damage is calculated by the softening function (Murray 2007) when strain energy terms (τ_b and τ_d) exceed the damage threshold (r_{0b} and r_{0d}), where ε_{max} is the maximum principal strain and ε_{ij} is the total strain components (Murray 2007).

The behavior of typical concrete shows nonlinearity and dilation before the peak strength. These behaviors are modeled using initial yield surface, $N_H F_f$, and back stress, α_{ij} . The translation of the yield surface is defined as back stress, which is denoted as α_{ij} . The value of each back stress component is zero at the initial yield and reaches the maximum value at ultimate strength. Initial yield surface hardens until it reaches the ultimate yield surface, F_f . The total stress is defined as the sum of initial yield strength and back stress, and the hardening rule is defined based on the α_{ij} as

$$\alpha_{ij}^{n+1} = \alpha_{ij}^n + \Delta \alpha_{ij}, \tag{10}$$

$$\sigma_{ij}^{Pn+1} = \sigma_{ij}^{KHn+1} + \alpha_{ij}^{n+1}, \tag{11}$$

where $\Delta \alpha_{ij}$ is incremental of back stress, σ_{ij}^{KH} is initial yield stress, and σ_{ij}^P is elastoplastic stress. Incremental of back stress is determined as

$$\Delta \alpha_{ij} = C_H G_\alpha \left(\sigma_{ij}^P - \alpha_{ij} \right) \Delta \dot{\varepsilon} \Delta t, \tag{12}$$

where C_H is a parameter to determine the rate of translation, G_α is a function that limits the increment of back stress, $\sigma_{ij}^P - \alpha_{ij}$ are the stress components that determine

the direction of translation, $\Delta\epsilon$ is effective strain rate increment, and Δt is the time step (Murray 2007).

3 Blast Wave

Blast waves are generated by explosive events that occur in an extremely short period. When the explosive explodes in the air, shock waves propagate along the discontinuous pressure front. Rapid release of a significant amount of energy instantaneously leads to an abrupt increase in pressure, and the pressure on the front gradually decreases as the distance from the explosion origin increases. After the pressure front has passed, the pressure behind the front drops exponentially and leads to a negative phase, which is less than the ambient atmospheric pressure. Explosive events affecting structures are primarily divided into unconfined and confined explosions. Unconfined explosions are classified as free air burst, airburst, and surface burst (U.S. Department of Defense 2008). Especially in the case of air burst and surface burst, the pressure at the front is amplified by interaction with the ground surface.

The characteristics of the blast wave are influenced by the physical properties of the medium in which the wave propagates. Criteria are needed to quantify blast loads to assess and predict the effect of the explosive on the structure. The properties of the explosion depend on the standoff distance and the amount of explosion, and the typical pressure–time history curve of the explosion is shown in Fig. 2 (U.S. Department of Defense 2008).

The cube-root scaling law using these two parameters is widely used, and the properties of blast load are

specified using the scaled distance Z . In the cube-root scaling law (Cranz 1917; Hopkinson 1915), the scaled distance Z is defined as

$$Z = \frac{D}{W^{\frac{1}{3}}}, \tag{13}$$

where D is the standoff distance, and W is the mass of the equivalent TNT. The scaled distance is used to quantify the characteristics of blast waves. When the scaled distance is determined, values of blast wave characteristics are obtained through the K–B curve (Kingery and Pannill 1964; Kingery 1966). The K–B curve was proposed by the US Army in the report of their Ballistic Research Laboratories (BRL). The K–B curve provides the parameters of blast waves such as pressure, impulse, duration, and other parameters of the blast environment as functions of scaled distance. The blast wave parameters are used for plotting the pressure–time curve and calculating peak overpressure for blast analysis and design.

4 Numerical Model

In order to evaluate the improvement of the blast load resistance capability of the Alfred Murrah building due to the application of HPCRCC, only the north frame directly destroyed by the explosion load is partially modeled. The structure from the 1st–5th floor between the column G16 and the column G24 is set as the target of the blast load. The model is constructed based on the detailed drawing and rebar configuration provided by FEMA 277 (Corley et al. 1996), as shown in Fig. 3, and shear reinforcements of columns and girders were not considered in this study. And the sectional geometries for columns

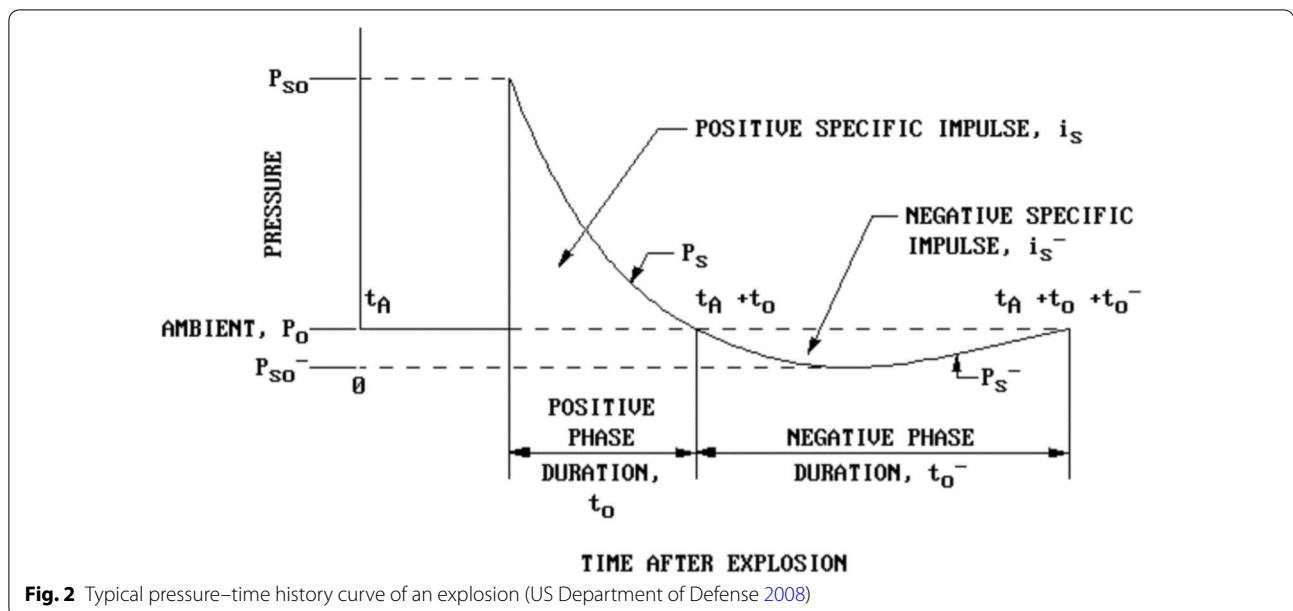
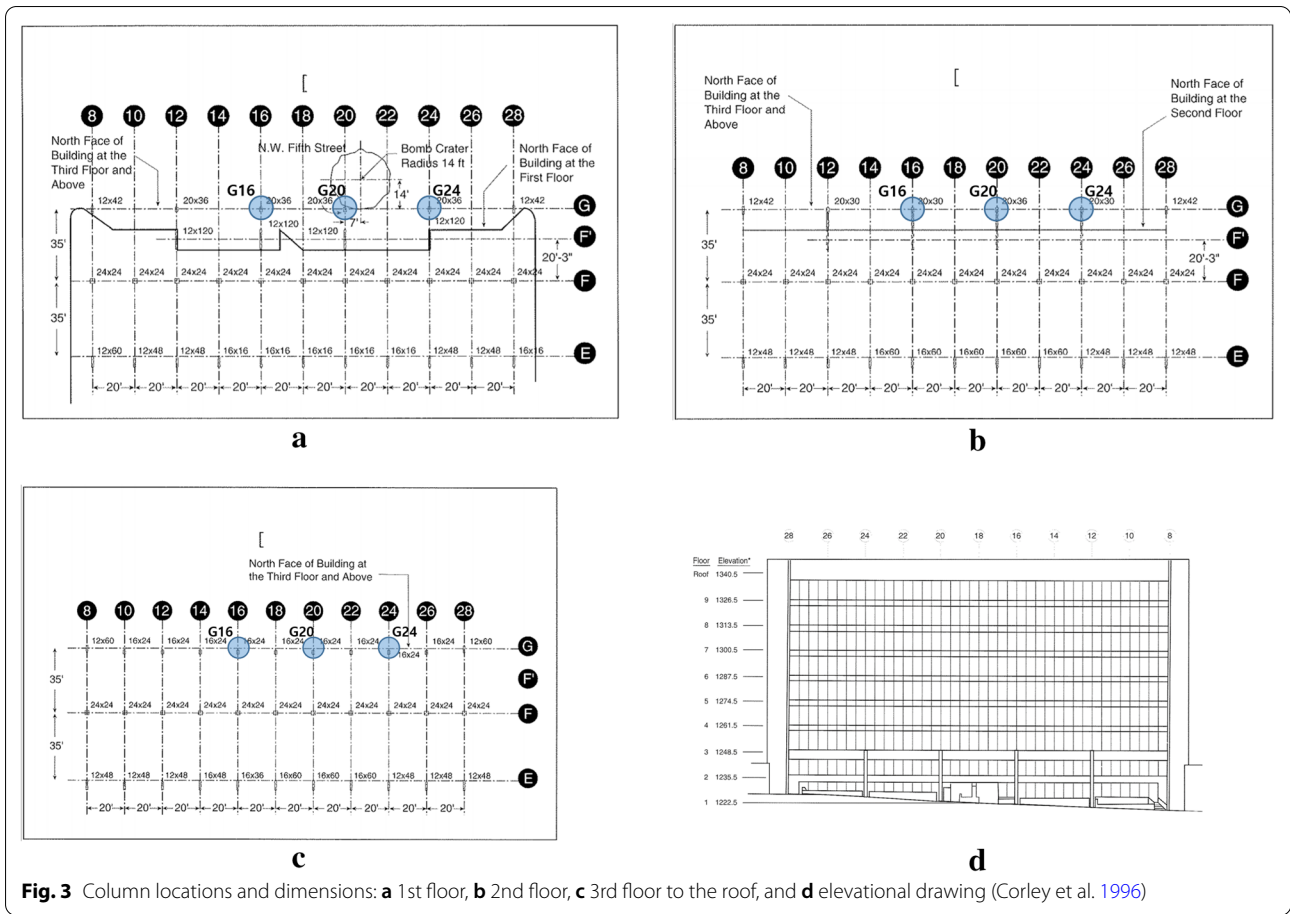


Fig. 2 Typical pressure–time history curve of an explosion (US Department of Defense 2008)



and girders, which are components of the target frame structure are shown in Fig. 4. Numerical models have been constructed considering the boundary conditions supporting the back of the frame since no detailed data has been disclosed other than the frame structure of the north side, which was published directly in the FEMA report (Corley et al. 1996). Because the drawings published in the report (Corley et al. 1996) basically use the English engineering unit system, the units used in Figs. 3 and 4 are feet and inch.

Eight numerical models are taken into consideration with differences in the reinforcement of HPCFRCC to evaluate the efficiency of the reinforcement (Table 1). The reinforcement is applied by sequentially replacing parts of the normal concrete to those of the HPCFRCC from the 1st to 5th floors by keeping the cross-section dimension and steel reinforcement ratio of each structural element. Only the concrete type is changed to investigate the utility of applying HPCFRCC.

Two types of material model are considered for the numerical frame model. As for steel rebar, a plastic kinematic material model is used. The plastic kinematic

model is used to simply describe hardening plasticity with strain rate effect. The CSCM material model is employed to describe the mechanical behavior of the normal concrete (27 MPa) and HPCFRCC (180 MPa). The CSCM model uses a viscoplastic algorithm to account for changes in material properties due to strain rate during high-speed deformation, and the plastic kinematic material model employs the Cowper–Symonds algorithm for accounting strain rate effect. The bond between two materials (rebar and concrete) parts is implemented using the keyword of ‘constrained_lagrange_in_solid’, which imposes the displacement of the nodes in the rebar to the adjacent nodes in the concrete part. The material properties of rebar are summarized in Table 2. The tensile strength of the CSCM model is determined by the yield surface (Fig. 2), and the Young’s modulus is determined by the following equation presented in the CEB-FIP model code (CEB-FIP 1990):

$$E = E_C \left(\frac{f'_c}{10} \right)^{1/3} \tag{14}$$

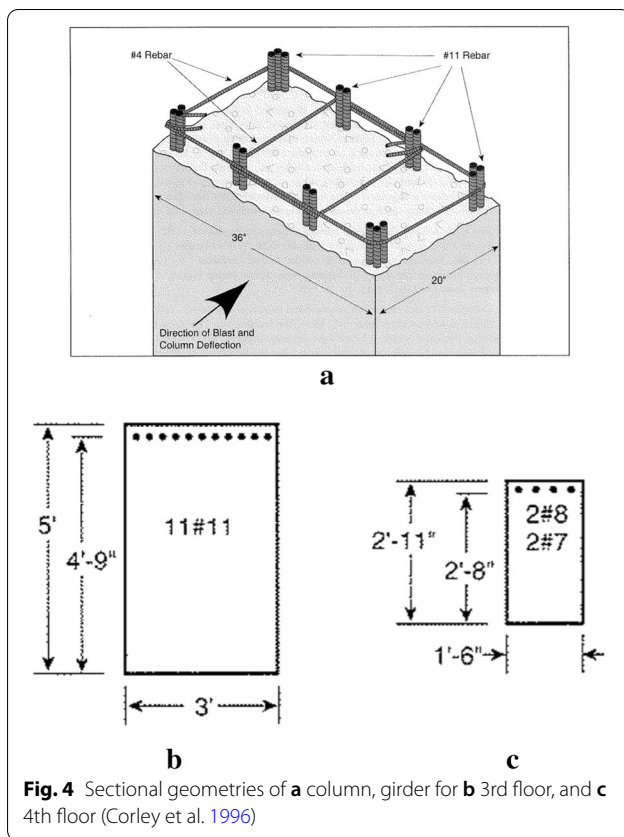


Fig. 4 Sectional geometries of **a** column, girder for **b** 3rd floor, and **c** 4th floor (Corley et al. 1996)

Table 1 Locations of reinforcement using HPRCC

| Model number | Location of HPRCC | |
|--------------|-------------------------------|--------------------------|
| | Column | Girder |
| 1 | None | None |
| 2 | 1st floor | None |
| 3 | 1st and 2nd floors | None |
| 4 | 1st and 2nd floors | 3rd floor |
| 5 | 1st, 2nd, and 3rd floors | 3rd floor |
| 6 | 1st, 2nd, and 3rd floors | 3rd and 4th floors |
| 7 | 1st, 2nd, 3rd, and 4th floors | 3rd and 4th floors |
| 8 | 1st, 2nd, 3rd and 4th floors | 3rd, 4th, and 5th floors |

The normal concrete and HPRCC parts consist of solid elements, and the rebar is composed of the beam elements, as shown in Fig. 5. The boundary condition is assumed where the bottom of the columns and the back of the beam–column joints are constrained, and the floor slabs are not considered in the numerical model. LS-Dyna is employed for the dynamic analysis of the frame

Table 2 Material properties material model

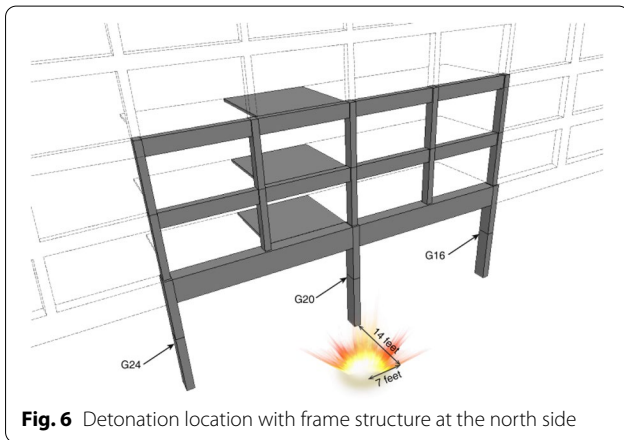
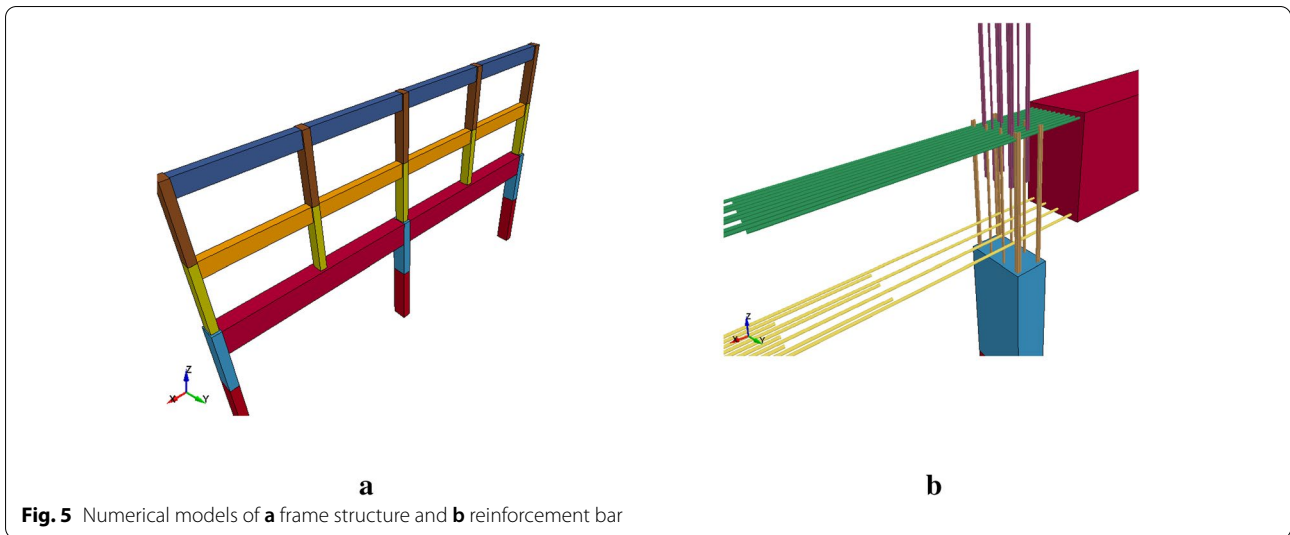
| Plastic kinematic material model (rebar) | |
|--|---------------------------------------|
| Young's modulus | 196.5 GPa |
| Poisson's ratio | 0.3 |
| Mass density | 7860 kg/m ³ |
| Yield strength | 413 MPa |
| Tangential modulus | 3.32 GPa |
| C (for Cowper–Symonds model) | 40.0 |
| P (for Cowper–Symonds model) | 5.0 |
| Failure strain | 0.3 |
| CSCM (normal concrete and HPRCC) | |
| Compressive strength | 27 MPa (concrete) and 180 MPa (HPRCC) |
| Mass density | 2400 kg/m ³ |
| IRATE | 1 |
| ERODE | 1.1 |

structure against blast pressure. Blast load is defined as a pressure function which is based on K–B curve with parameters of equivalent TNT mass, the location of the detonation point, characteristics of explosion load (free air burst, airburst, and surface reflection condition). Specifically, 2 tons of TNT mass is taken into consideration. The height of the detonation is 1.37 m (4.5 ft) from the ground, and the bomb center is located at 4.77 m (15.65 ft) away from the column G20 with surface reflection, as shown in Fig. 6.

5 Numerical Results

Blast analyses of the eight numerical models are performed by the detonation of 2 tons of TNT, which is equivalent to the amount used in the Oklahoma City bombing. The damage distributions and the deformed shapes are presented in Figs. 7, 8, 9, 10, 11, 12, 13 and 14, and the damage contour represent the maximum value of brittle and ductile damage (Eqs. (8) and (9)) in each element.

In the numerical results of Model 1 using the normal concrete under the same conditions as the actual building, most of the structural elements between the G20 and G24 columns and below the 4th floor are destroyed with the greatest damage in the girder on the 3rd floor, consistent with the Oklahoma City bombing. In the case of reinforcement with HPRCC only on the 1st-floor columns (Model 2), there is no significant difference from the normal concrete structure (Model 1). This is because



even though the columns on the 1st and 2nd floor are replaced with HPCRCC, column G20, which is the closest member, cannot resist the blast load.

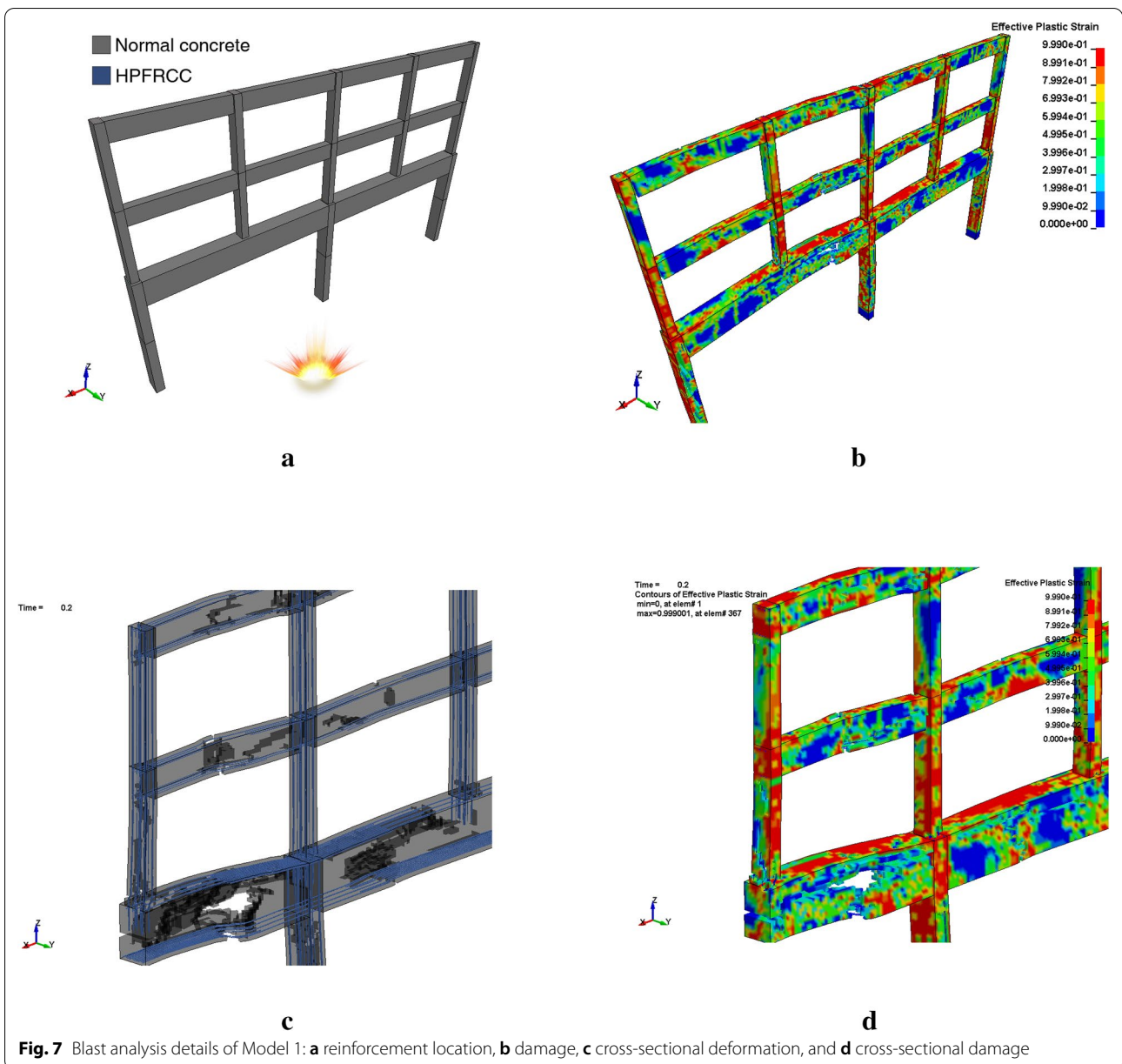
The damage on the 1st and 2nd-floor columns is significantly reduced compared with that of the normal concrete structure (Model 1), and only local damage is observed in the case of Model 3 (1st and 2nd floor are reinforced with HPCRCC). However, the girder on the 3rd floor is destroyed the same as that of Model 1 and 2.

In the case of Model 4 (columns on the 1st and 2nd floors and the 3rd-floor girders are reinforced), serious destruction is not observed, but the considerable damage remains on the 3rd-floor columns.

In the numerical model where the 1st to 3rd-floor columns and the 3rd-floor girder are reinforced (Model 5), destruction of the 3rd-floor girder does not occur, and the damage to the columns on the 3rd floor is also considerably reduced. However, as the lower floors become stiffer, the blast energy is not absorbed by the deformation energy of the lower floors, and the girder of the upper floor (5th floor) fails. This phenomenon might be prevented by reinforcing the girders of the 4th and 5th floors (Models 6–8). In conclusion, the reinforcement of the girder is more important than that of columns in 3rd and higher floors, and at least columns of the 1st to 3rd floors and girders of 3rd to 5th floors should be reinforced to prevent structural destruction.

The responses at girders on the 3rd and 4th floors increase even though the parts on lower floors are replaced with HPCRCC. The reinforcement of the girders on the 3rd and 4th floors significantly improves the resisting capacity of the structures.

In terms of maximum displacement at specific locations (Fig. 15 and Table 3), the reinforcement needs to be carefully determined so that the structure efficiently improves resisting capacity. The displacements are relative from the ground in the y-direction (in Fig. 5). The maximum displacement of the 3rd-floor girder decreases significantly as the columns at the 1st and 2nd floors are reinforced by HPCRCC. However, the maximum displacement of the 4th-floor girder increases even though the members at the lower floor are reinforced. It appears



that the blast energy, which is transferred to the strain energy of the lower structural parts of the normal concrete frame (Model 1), leads to the more substantial deformation of the upper structural parts rather than the lower parts when members on lower floors are reinforced with the stiffer material than normal concrete (Model 2–4).

6 Conclusions

In this research, we evaluate the blast resistance of a frame structure reinforced by HPFRCC. The Alfred Murrah building, which experienced a terrorist attack in 1995, is selected as a target structure, and the northern frame structure directly affected by the blast load

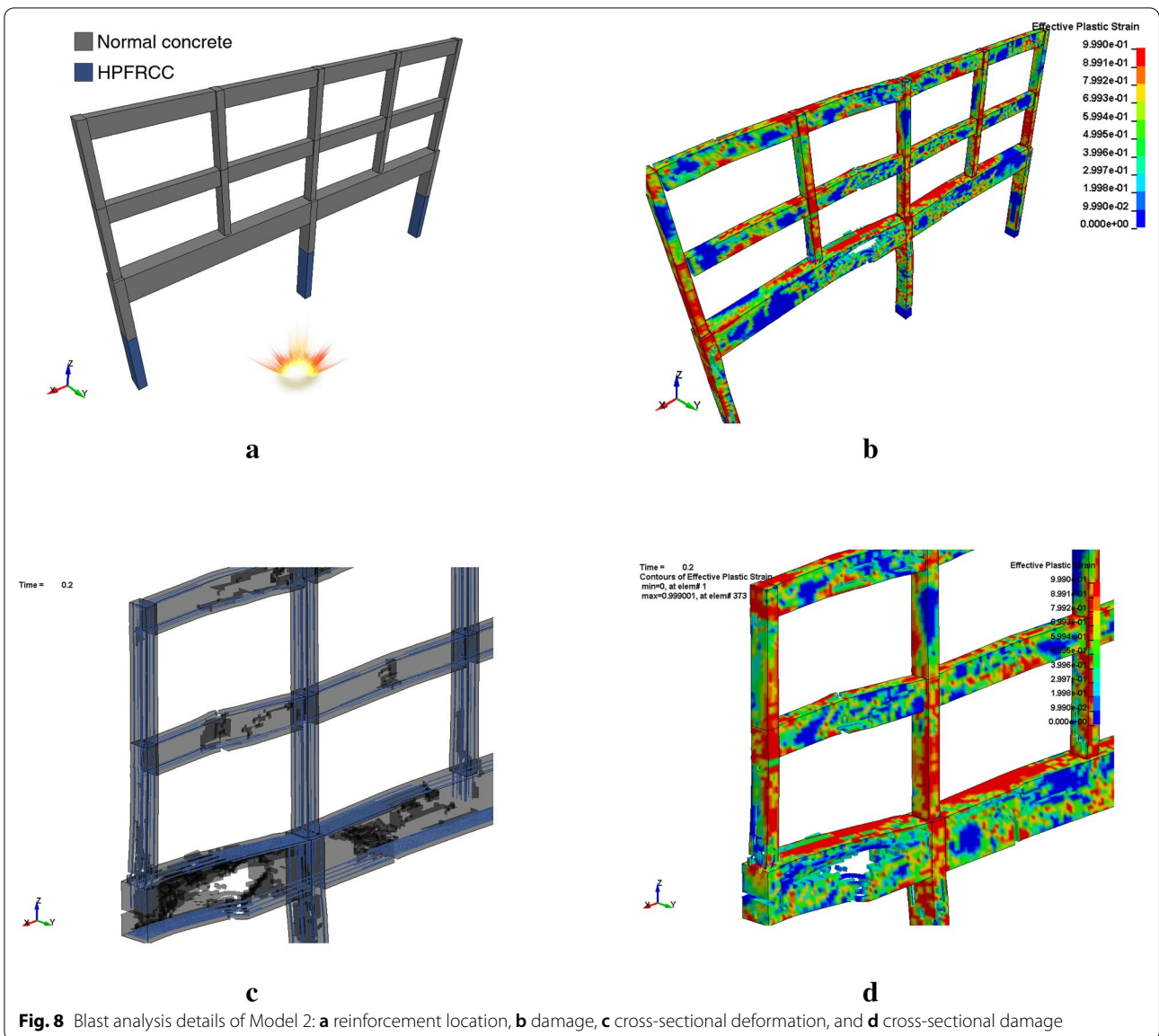
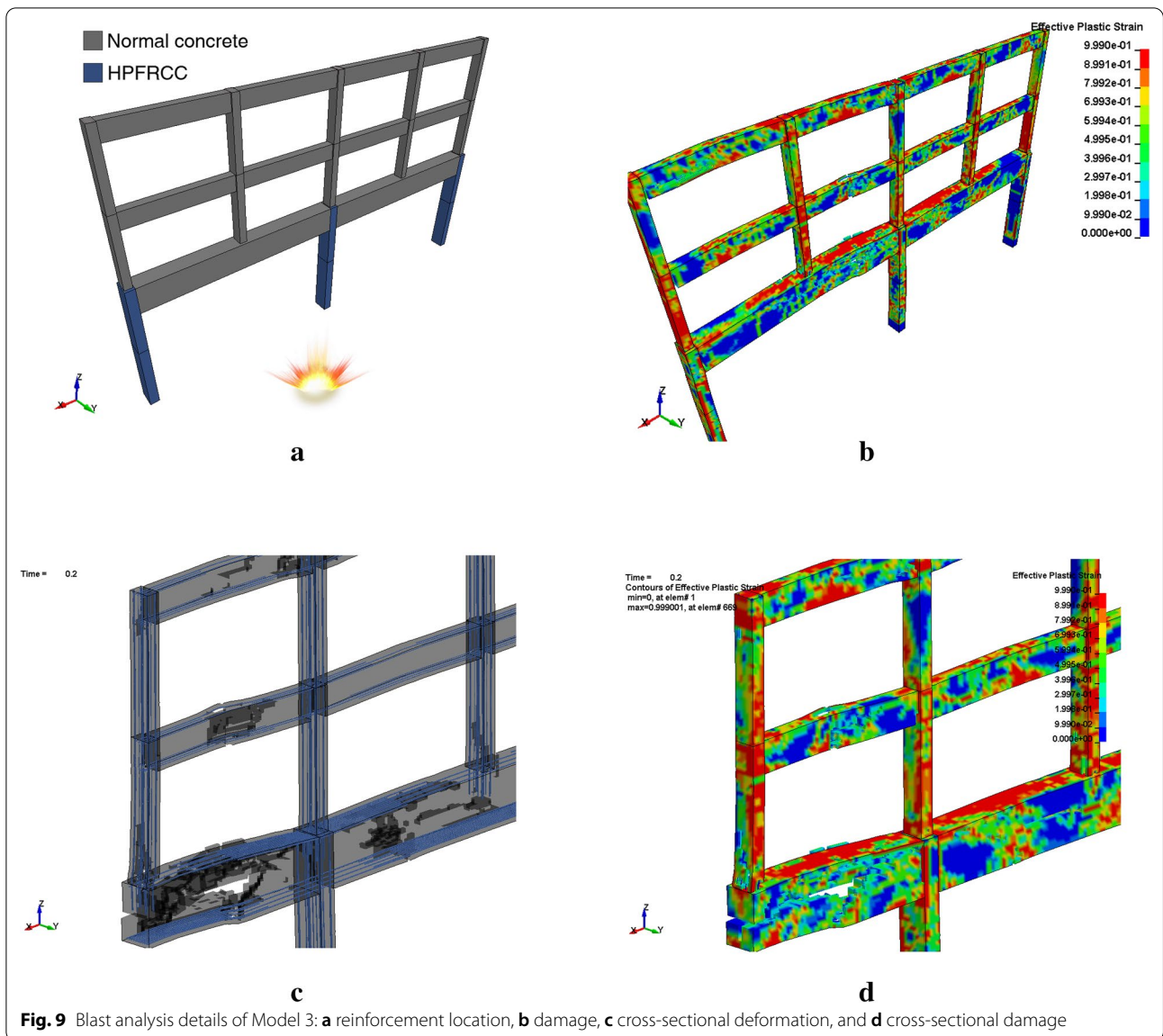


Fig. 8 Blast analysis details of Model 2: **a** reinforcement location, **b** damage, **c** cross-sectional deformation, and **d** cross-sectional damage

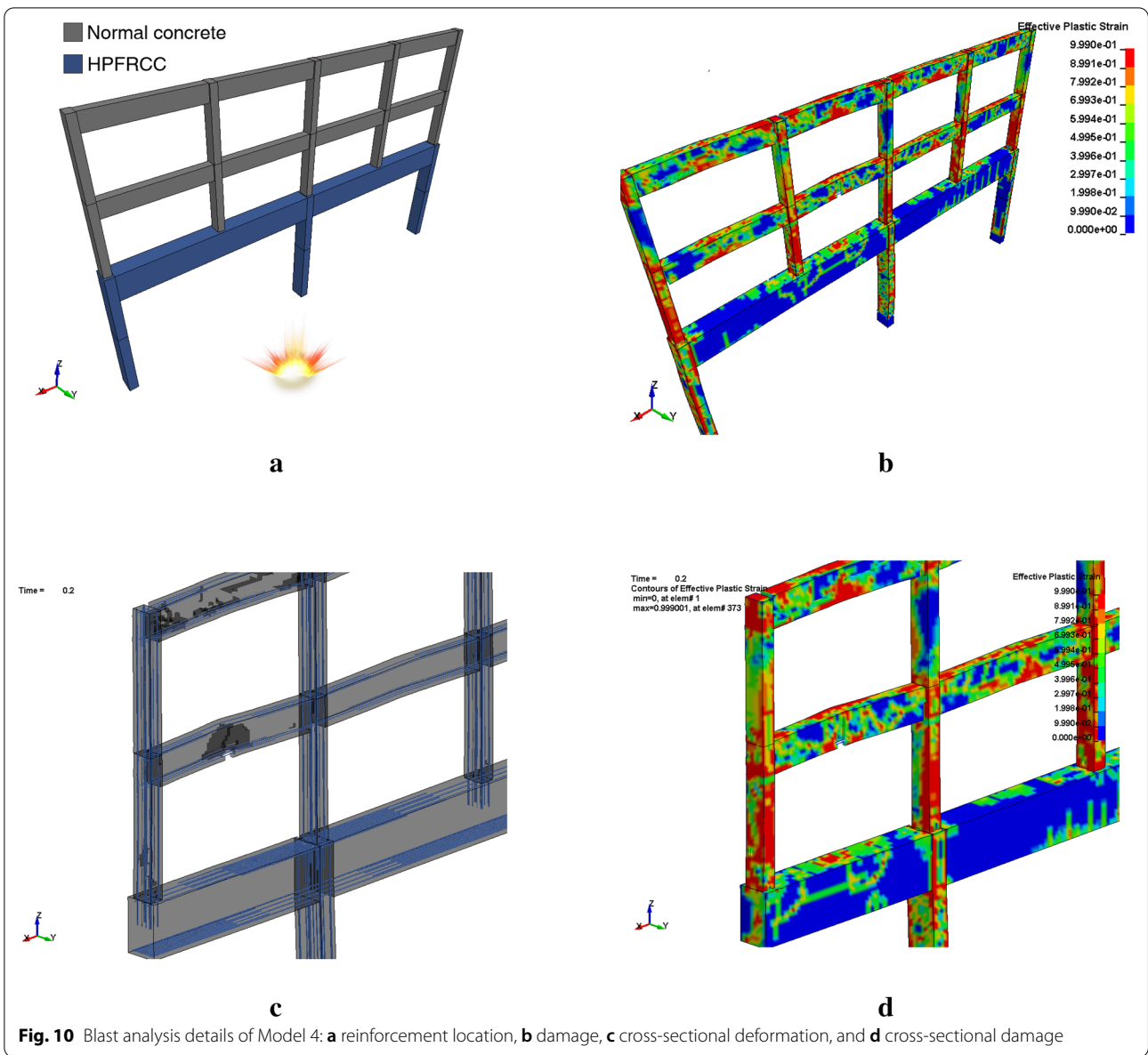
is considered for the blast analysis. The blast response of the structure is evaluated through the finite element method. The CSCM model is used to describe the behavior of normal concrete and HPFRCC, and it is confirmed that the reinforcement reduces the damage and improves resistance to deformation. Eight numerical frame models are constructed considering various reinforcing methods by sequentially replacing normal concrete members with HPFRCC members.

Additionally, the effectiveness of the various reinforcement methods is evaluated. We determined that it is essential to reinforce the columns and girders of the lower floors exposed to large blast loads. In particular, in the high-rise part, the girders should be reinforced rather than the columns to resist the blast load effectively. Terrorist attacks on civilian structures result in many human, social and economic losses. The reinforcement of civilian structures using the latest



materials, whose properties have not yet been clarified, has many limitations. It is important not only in engineering, but also socially to confirm the blast-resistance

performance of structures using HPFRCC, the latest material, whose behavior has not been clearly identified, and to suggest reinforcement methods.



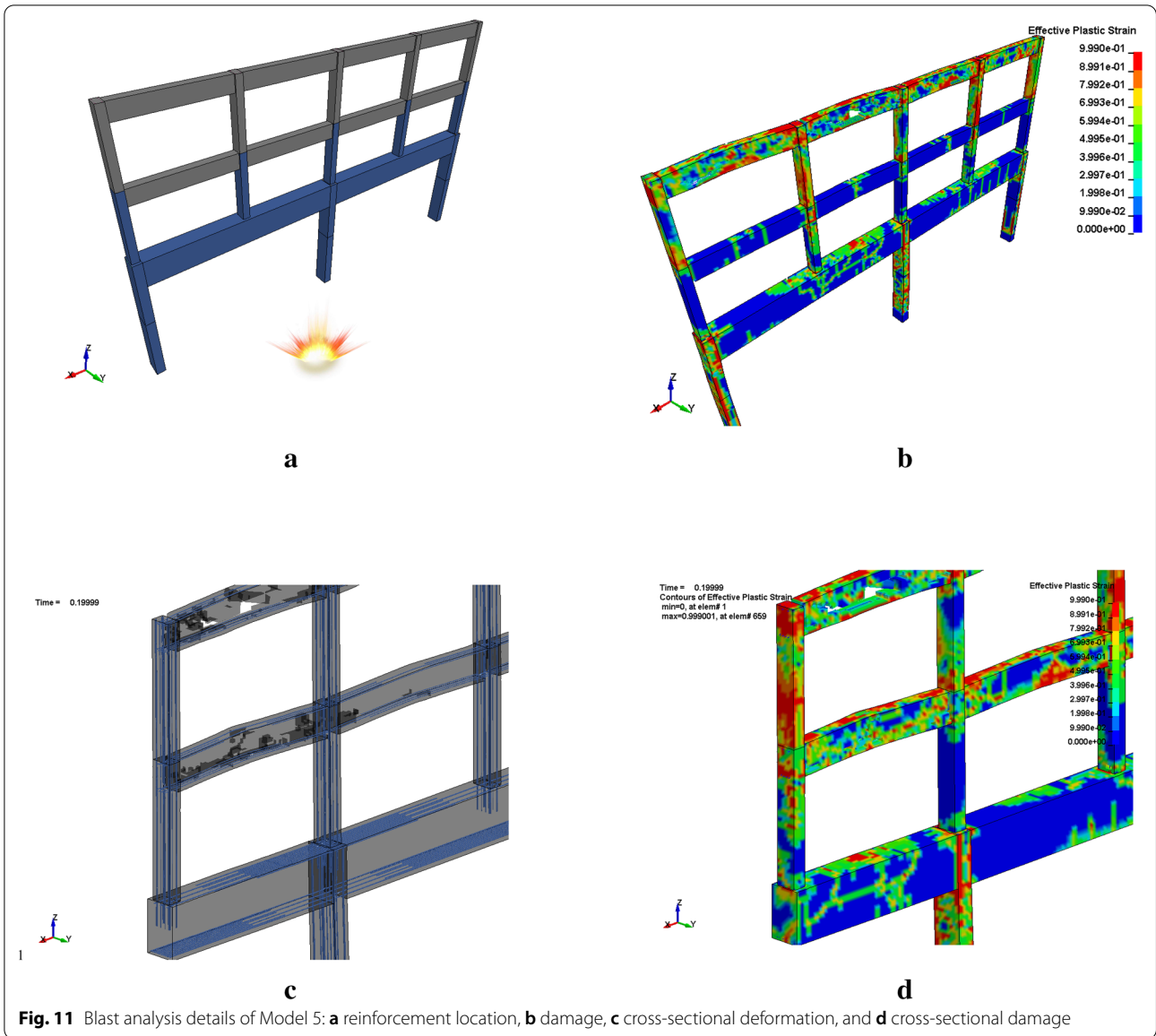


Fig. 11 Blast analysis details of Model 5: **a** reinforcement location, **b** damage, **c** cross-sectional deformation, and **d** cross-sectional damage

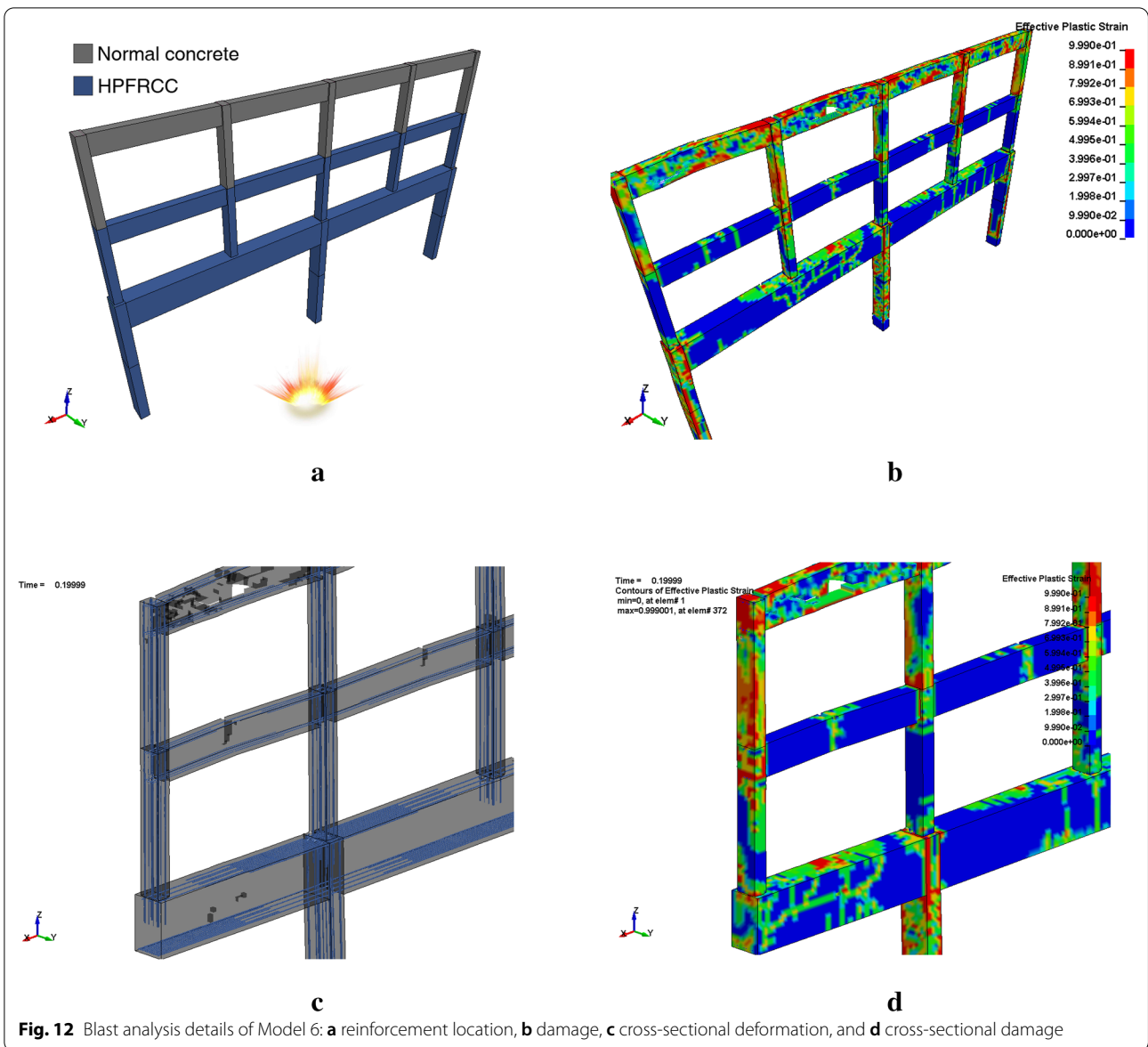


Fig. 12 Blast analysis details of Model 6: **a** reinforcement location, **b** damage, **c** cross-sectional deformation, and **d** cross-sectional damage

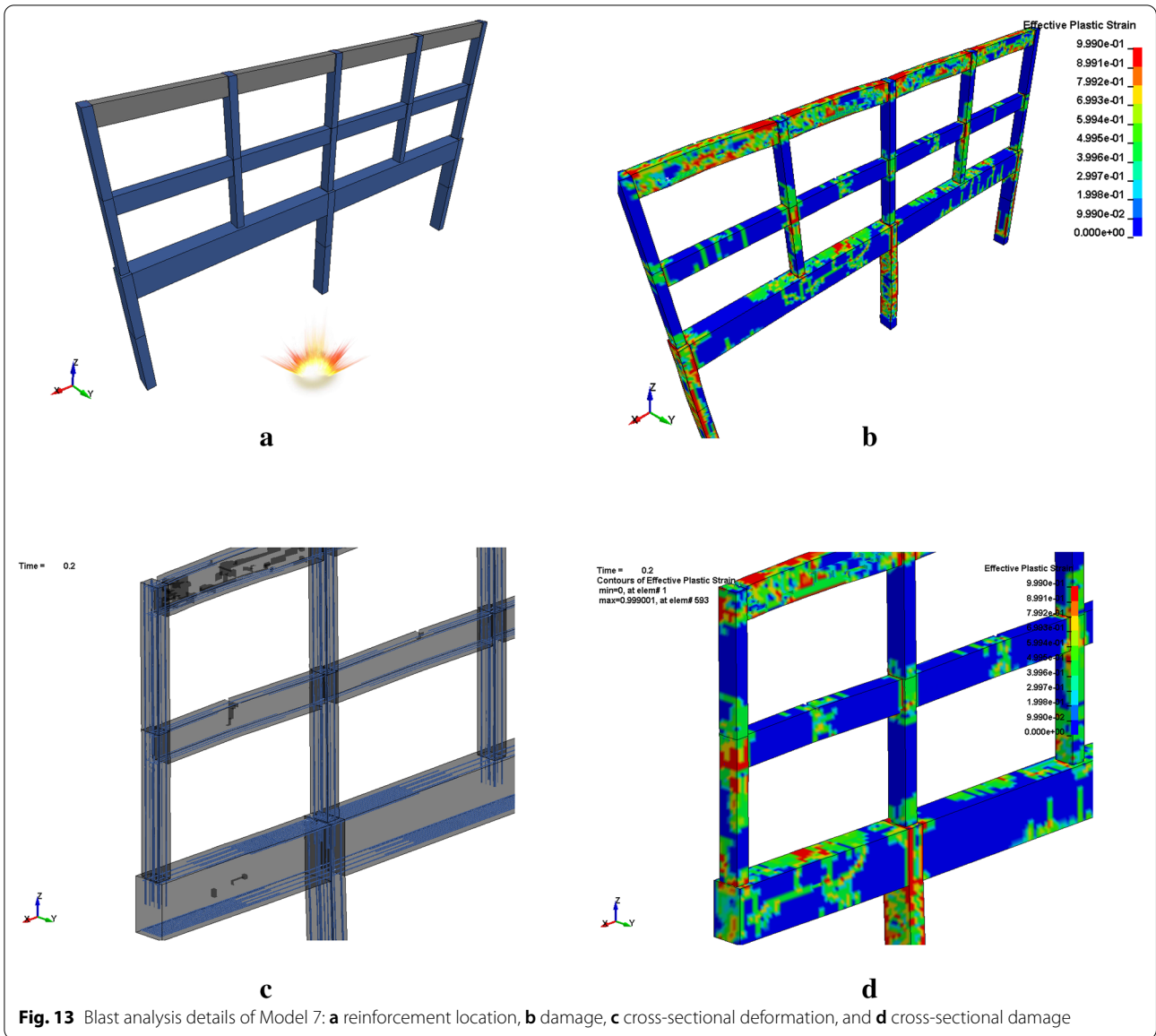


Fig. 13 Blast analysis details of Model 7: **a** reinforcement location, **b** damage, **c** cross-sectional deformation, and **d** cross-sectional damage

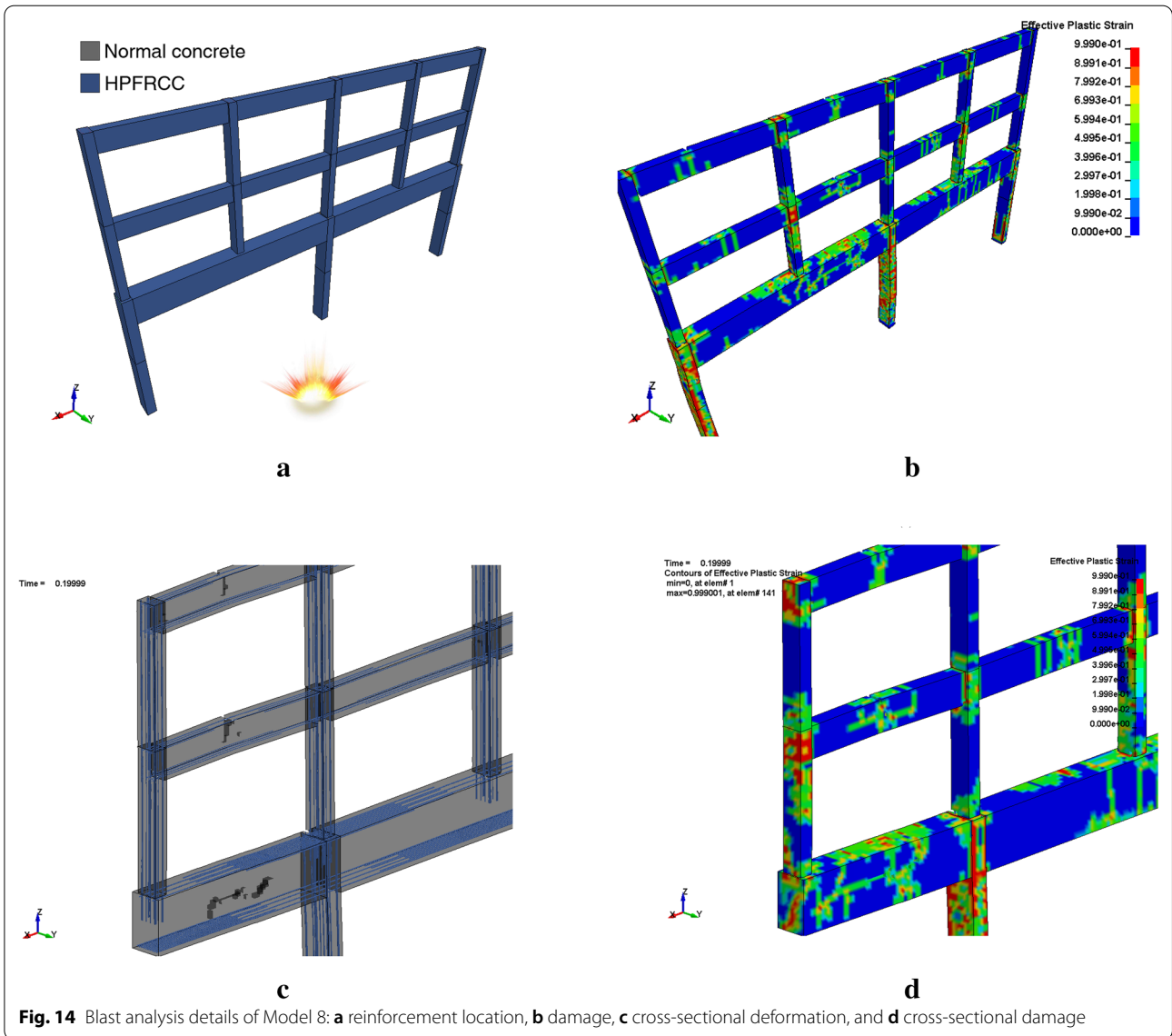


Fig. 14 Blast analysis details of Model 8: **a** reinforcement location, **b** damage, **c** cross-sectional deformation, and **d** cross-sectional damage

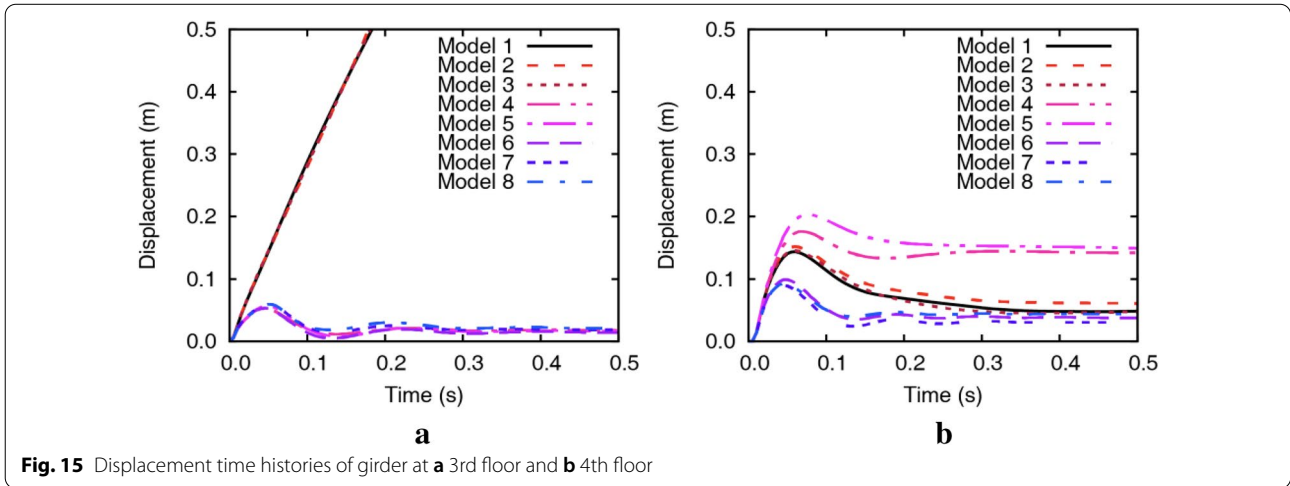


Fig. 15 Displacement time histories of girder at **a** 3rd floor and **b** 4th floor

Table 3 Maximum displacement at girder

| Model | Displacement of 3rd floor | Displacement of 4th floor |
|---------|---------------------------|---------------------------|
| Model 1 | Fail | 0.144 m |
| Model 2 | Fail | 0.152 m |
| Model 3 | Fail | 0.145 m |
| Model 4 | 0.053 m | 0.176 m |
| Model 5 | 0.057 m | 0.203 m |
| Model 6 | 0.053 m | 0.099 m |
| Model 7 | 0.059 m | 0.090 m |
| Model 8 | 0.060 m | 0.092 m |

Acknowledgements

This work was supported by the National Research Foundation of Korea (NRF) grant funded by the Korea government (MSIT) (No. 2018R1A2A1A05019453), and was also supported by the National Research Foundation of Korea (NRF) grant funded by the Korea government (NRF-2017M2A8A4014829).

Authors' contributions

J.W. Jung conducted numerical simulations and analyzed the results. J.W. Hong is a major contributor in writing the manuscript. All authors read and approved the final manuscript.

Authors information

Jae-Wook Jung is a Senior Researcher in the Structural Safety & Prognosis Research Division, Korea Atomic Energy Research Institute, Daedeok-daero 989-111, Yuseong-gu, Daejeon, Republic of Korea.

Jung-Wuk Hong is a Professor in the Department of Civil and Environmental Engineering, Korea Advanced Institute of Science and Technology, 291 Daehak-ro, Yuseong-gu, Daejeon, Republic of Korea.

Funding

This work was supported by the National Research Foundation of Korea (NRF) Grant funded by the Korea government (MSIT) (No. 2018R1A2A1A05019453), and was also supported by the National Research Foundation of Korea (NRF) Grant funded by the Korea government (NRF-2017M2A8A4014829).

Availability of data and materials

The datasets used and/or analyzed during the current study are available from the corresponding author on reasonable request.

Competing interests

The authors declare that they have no competing interests. The authors declare that they have no competing interests.

Author details

¹ Structural Safety & Prognosis Research Division, Korea Atomic Energy Research Institute, Daedeok-daero 989-111, Yuseong-gu, Daejeon 34057, Republic of Korea. ² Department of Civil and Environmental Engineering, Korea Advanced Institute of Science and Technology, 291 Daehak-ro, Yuseong-gu, Daejeon 34141, Republic of Korea.

Received: 12 March 2020 Accepted: 9 October 2020

Published online: 02 February 2021

References

- Bathe, K.-J. (2006). *Finite element procedures*. Klaus-Jurgen Bathe.
 Caverzan, A., Cadoni, E., & Di Prisco, M. (2012). Tensile behaviour of high performance fibre-reinforced cementitious composites at high strain rates. *International Journal Of Impact Engineering*, 45, 28–38. <https://doi.org/10.1016/j.ijimpeng.2012.01.006>.

- CEB-FIP, M. C. (1990). Design code. *Comite Euro International du Beton*, 51–59.
- Choi, W.-C., Yun, H.-D., Cho, C.-G., & Feo, L. (2014a). Attempts to apply high performance fiber-reinforced cement composite (HPFRCC) to infrastructures in South Korea. *Composite Structures*, 109, 211–223. <https://doi.org/10.1016/j.compstruct.2013.10.027>.
- Choi, Y.-W., Choi, B.-K., Park, M.-S., & Sung, D. (2014). A study on the rheology properties for development of sprayed high performance fiber reinforced cementitious composites for protection and blast resistant. *Journal of the Korean Recycled Construction Resources Institute*, 2(3), 188–195. <https://doi.org/https://doi.org/10.14190/JRCR.2014.2.3.188>
- Corley, W. G., Sozen, M. A., Thornton, C. H., & Mlakar, P. F. (1996). *The Oklahoma City bombing: Improving building performance through multi-hazard mitigation*. Federal Emergency Management Agency Mitigation Directorate, FEMA Report (Vol. 277).
- Cranz, C. (1917). *Lehrbuch der ballistik* (Vol. 2). Рипол Классик.
- Hallquist, J. O. (2007). *LS-DYNA keyword user's manual*. Livermore Software Technology Corporation (Vol. 970).
- Hopkinson, B. (1915). *British ordnance board minutes 13565*. The National Archives (Vol. 13565). Kew, UK.
- Jung, J.-W., Yoon, Y.-C., Jang, H. W., & Hong, J.-W. (2019). Investigation on the resistance of steel-plate concrete walls under high-velocity impact. *Journal of Constructional Steel Research*, 162, 105732.
- Kazemi-Moghaddam, A., & Sasani, M. (2015). Progressive collapse evaluation of Murrah Federal Building following sudden loss of column G20. *Engineering Structures*, 89, 162–171. <https://doi.org/10.1016/j.engstruct.2015.02.003>.
- Khosravani, M. R., Nasiri, S., Anders, D., & Weinberg, K. (2019). Prediction of dynamic properties of ultra-high performance concrete by an artificial intelligence approach. *Advances in Engineering Software*, 127, 51–58.
- Kingery, C N, & Pannill, B. F. (1964). *Peak overpressure vs scaled distance for TNT surface bursts (hemispherical charges)*. ARMY BALLISTIC RESEARCH LAB ABERDEEN PROVING GROUND MD.
- Kingery, Charles N. (1966). *Air blast parameters versus distance for hemispherical TNT surface bursts*. ARMY BALLISTIC RESEARCH LAB ABERDEEN PROVING GROUND MD.
- Kosa, K., Naaman, A. E., & Hansen, W. (1991). Durability of fiber reinforced mortar. *Materials Journal*, 88(3), 310–319.
- Murray, Y. D. (2007). *Users manual for LS-DYNA concrete material model 159*.
- Ren, L., Yu, X., He, Y., Wang, K., & Yao, H. (2020). Numerical investigation of lateral inertia effect in dynamic impact testing of UHPC using a Split-Hopkinson pressure bar. *Construction and Building Materials*, 246, 118483.
- Simo, J. C., & Ju, J. W. (1987). Strain-and stress-based continuum damage models—II. Computational aspects. *International journal of solids and structures*, 23(7), 841–869.
- Tran, T. K., & Kim, D. J. (2014). High strain rate effects on direct tensile behavior of high performance fiber reinforced cementitious composites. *Cement and Concrete Composites*, 45, 186–200. <https://doi.org/10.1016/j.cemconcomp.2013.10.005>.
- U.S. Department of Defense. (2008). *Structures to resist the effects of accidental explosions*. UFC 3–340–02.
- Yin, H., Shirai, K., & Teo, W. (2019). Numerical simulation of the blast-resistant response of ultrahigh-performance concrete structural members. *Journal of Civil Engineering and Management*, 25(6), 587–598.
- Yin, H., Shirai, K., & Teo, W. (2019). Finite element modelling to predict the flexural behaviour of ultra-high performance concrete members. *Engineering Structures*, 183, 741–755.

Publisher's Note

Springer Nature remains neutral with regard to jurisdictional claims in published maps and institutional affiliations.